Nanobioanalysis

DOI: 10.1002/ange.201404744

Nanoelectrode for Amperometric Monitoring of Individual Vesicular Exocytosis Inside Single Synapses**

*Yu-Tao Li, Shu-Hui Zhang, Li Wang, Rong-Rong Xiao, Wei Liu, Xin-Wei Zhang, Zhuan Zhou, Christian Amatore, and Wei-Hua Huang**

Abstract: *Chemical neurotransmission occurs at chemical synapses and endocrine glands, but up to now there was no means for direct monitoring of neurotransmitter exocytosis fluxes and their precise kinetics from inside an individual synapse. The fabrication of a novel finite conical nanoelectrode is reported perfectly suited in size and electrochemical properties for probing amperometrically inside what appears to be single synapses and monitoring individual vesicular exocytotic events in real time. This allowed obtaining direct and important physiological evidences which may yield important and new insights into the nature of synaptic communications.*

Vesicular exocytosis is a fundamental process for interneuronal or neuromuscular communications as well as for the endocrine glands.[1] Chemical neurotransmitters are transported intracellularly within vesicles and their release involves fusion of the vesicle and cell membranes triggered by Ca^{2+}. The major importance of vesicle traffic and cargo transport in cells has been well recognized by the award of the 2013 Nobel Prize in Physiology or Medicine jointly to J. E. Rothman, R. W. Schekman, and T. C. Südhof for their seminal discoveries of the relevant transport mode regulations and machineries.[2] However, much less is known about the mechanisms commanding and regulating the ultimate stage through which the messengers are delivered into the extracellular medium, in particular when this occurs in extremely narrow synaptic clefts.[3] The biggest obstacle up to now has been due to the lack of accurate tools for highly sensitive monitoring in real time extremely small neurotransmitters fluxes released inside nanometric synaptic gaps.

Amperometry at carbon fiber microelectrodes (CFMEs) creates an artificial synaptic cleft configuration in which the target cell is replaced by a Faradaic ultra-microelectrode at which each released messenger molecule is oxidized so that released fluxes are directly converted into electrical currents.[4] To date, amperometry using "artificial synapse" configuration provided a wealth of information regarding the final outcome of vesicles release through precise quantification and kinetic characterization of individual exocytotic events. However, in "artificial synapses", there is not any possible feedback regulation between cells.[5] Though this is not a key issue for endocrine cells, neurotransmitter release in real synapses involves feedback between postsynaptic and presynaptic active zones which are facing each other across synaptic clefts.[6] Therefore, direct probing inside individual synapses with real-time monitoring of neurotransmitter fluxes therein is required for understanding the nature of the chemical neurotransmission in neuronal systems.

To achieve such goal, amperometry at carbon fiber nanometric electrodes (CFNEs) seems the most promising method because of the excellent time and space resolution. However, CFNEs shapes must be adapted in order to be slipped into synaptic clefts without destroying the local biological structures. Although great advances have been achieved in nanofabrication and use of nanometer-sized electrochemical sensors for measurements near or inside cells,[7] it is still a great challenge to routinely fabricate extremely small electrochemical probes with high performance.[8] This explains why no means have been proposed so far for direct monitoring of neurotransmitter exocytotic release inside individual synapses.

Herein we wish to disclose the fabrication of a novel CFNE suited for monitoring individual exocytotic events in real time within what appears to be single synapses based on the presented evidences (Figure 1, 2). Conical CFNEs were fabricated by sealing flame-etched carbon fibers inside glass nanopipettes (Figure 1) so as to expose active conical nanotips with dimensions allowing sliding them between two neurons membranes, namely, inside the space between neuron varicosities and their underlying soma (Figure 2) to enable amperometric detection of exocytotic events occurring therein. All independent tests presented hereafter concur to the fact that this allowed the first direct and in situ measurements of crucial features of release mechanism inside neural synapses.

[*] Y. T. Li,[+] S. H. Zhang,[+] R. R. Xiao, X. W. Zhang, Prof. W. H. Huang
Key Laboratory of Analytical Chemistry for Biology and Medicine (Ministry of Education)
College of Chemistry and Molecular Sciences
Wuhan University, Wuhan 430072 (China)
E-mail: whhuang@whu.edu.cn
Dr. L. Wang, W. Liu, Prof. Z. Zhou
Institute of Molecular Medicine, Peking University
Beijing 100871 (China)
Prof. C. Amatore
Ecole Normale Supérieure, Département de Chimie, UMR 8640 (CNRS-ENS-UPMC and LIA CNRS-XiamENS)
24 rue Lhomond, 75005 Paris (France)
[+] These authors contributed equally to this work.

[**] Supported by the National Natural Science Foundation of China (grant numbers 21375099, 91017013), Doctoral Fund of Ministry of Education of China (grant number 20120141110031), the Program for Changjiang Scholars and Innovative Research Team in University (IRT1030), the Fundamental Research Funds for the Central Universities (grant number 2042014kf0192), UMR 8640 (CNRS-ENS-UPMC) and LIA CNRS XiamENS.

Supporting information for this article is available on the WWW under http://dx.doi.org/10.1002/anie.201404744.

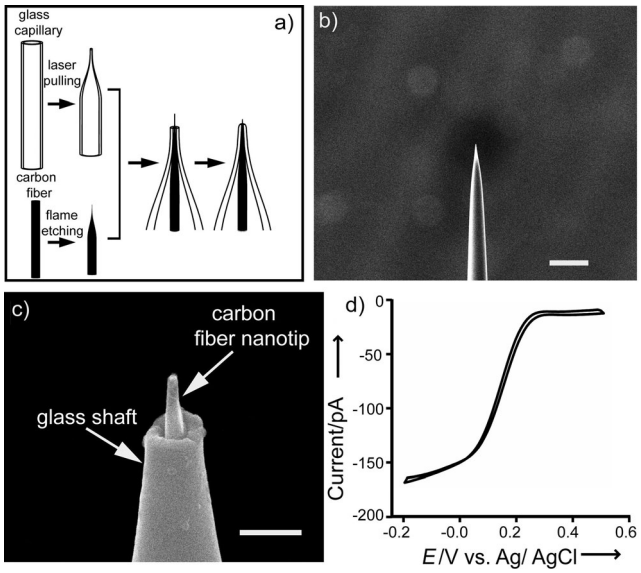

Figure 1. Fabrication and characterization of CFNEs. a) Schematic diagram showing main process for fabrication of conical CFNEs, a glass capillary was pulled to form a glass sub-micropipette, and a 7 μm radius carbon fiber was flame etched to form a needle shape nanotip. The etched carbon fiber was then inserted into the sub-micropipette and then fused. b) Global view (scanning electron microscopy) of a conical CFNE showing its shaft; the scale bar is 100 μm. c) Amplified picture of its tip; the scale bar is 1 μm. d) Cyclic voltammogram from a conical CFNE in 1 mmol L^{-1} potassium ferricyanide.

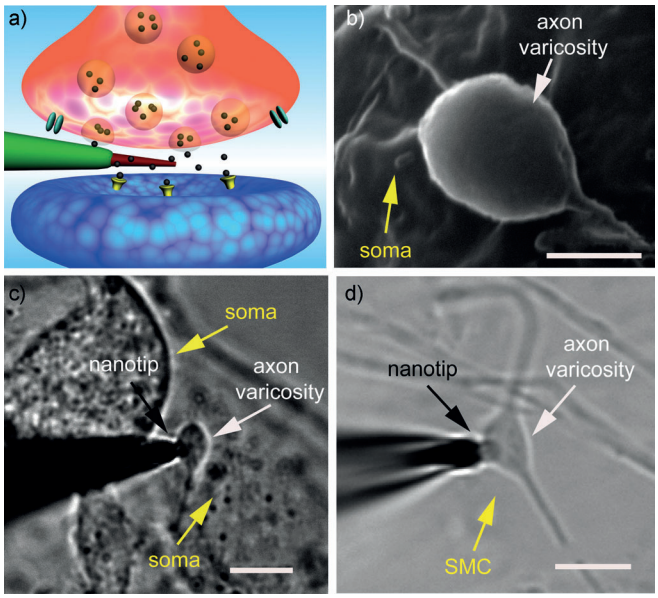

Figure 2. a) Schematic representation of a nanosensor's tip inside an individual synapse. b) SEM pictures showing a synapse formed between cultured superior cervical ganglion (SCG) sympathetic neurons; the scale bar is 1 μm. c,d) Bright-field photomicrographs showing the tip of a sensor inside a synapse between a varicosity of a SCG neuron and the soma of another SCG neuron (c), and inside a synapse between a varicosity of a SCG neuron and smooth muscle cell (d); the scale bars are 5 μm.

The facile and robust technique developed to routinely fabricate CFNEs combined flame-etching procedure[7a,9] with glass-pulled nanopipettes microfabrication. These were used to seal and insulate flame-etched carbon nanofibers (Figure 1 a) so as leaving only a protruding cone-shaped CFNEs with 50–200 nm tip diameter and 500–2000 nm shaft length (Figure 1 b). Further etching with a microforge yielded very fine conical tips with base radii, a, less than 100 nm and controlled shaft lengths, h, less than 1 μm (Figure 1 c) with high-aspect ratio $H = h/a \approx 7$. The nanotips showed excellent electrochemical characteristics and large sensitivity. Calibrations with 1 mM ferrocyanide ($D = 7.6 \times 10^{-6}$ $cm^2 s^{-1}$) afforded limiting current plateaus of approximately 0.15 nA (Figure 1 d) consistent with the 0.17 nA theoretical value predicted by the equation $i_{lim}^{cone} = 4FDca(1+qpH)$ for steady-state diffusion at conical electrodes,[10] where $q = 0.30661$, and $p = 1.14466$, F being the Faraday constant, and D and c the diffusion coefficient and bulk concentration of the redox probe. The fabrication process was well-controlled and reproducible with a success rate over 75% (550 CFNEs; Figure S1). The average capacitance and root-mean-square (rms) noise of these electrodes were 0.55 ± 0.24 pF and 460 ± 115 fA (mean $\pm$ sd, $n = 15$), demonstrating the excellent seal quality between glass shafts and conical carbon nanofibers.

The capability of these CFNEs for electrochemical monitoring of neurotransmitter vesicular release was tested using chromaffin cells and compared to usual 5 μm diameter CFMEs. In both cases, well-defined amperometric spikes were recorded, provided the CNFEs were positioned with their cone shaft touching the cell surface (CFMEs: Figure S2a; CFNEs: Figure S2b). Though having a much smaller surface area (ca. 3–4%) than the CFMEs, high detection probabilities (ca. 21% vs. CFMEs) were obtained at CFNEs (Figure S2b) evidencing the gain in collection because of fast side diffusion of neurotransmitters towards the nanometric conical surface.[11] These results thus demonstrated that albeit their different sizes and different manufacturing procedures, CFNEs and CFMEs displayed similar properties for real-time monitoring of neurotransmitter release.

Previous studies showed that sympathetic neurons in culture formed complex interconnecting networks and synapses by numerous axonal varicosities.[12] Quantal release of norepinephrine (NE) from superior cervical ganglion (SCG) neurons has also been electrochemically detected by placing CFMEs above clusters of SCG cells or varicosities.[12b,13] This encouraged us to let isolated SCG neurons interconnect and build synapses (Figure S3) while observing completion of these phases with a 100× oil immersion objective (Figure S4). CFNEs could then be carefully slipped inside individual synapses (Figure S5 and Movie S1) for amperometric monitoring.

For our purpose here we first wished to ensure that the synapses were not destroyed, that is, properly sealed back after CFNEs were positioned inside them and that CNFEs insertion did not altered the electrochemically active surface. To test for these critical issues we performed a series of controls based on the biocompatible $[Ru(NH_3)_6]^{2+/3+}$ redox pair and evaluated its limiting currents at different insertion depths inside the synapses.[7d] Figure S6 exemplifies that the

$Ru^{II/III}$ currents dropped to ca. 50% of their values outside the synapse after half-insertion of the active nanotips and down to ca. 7% after complete insertion, indicating a satisfactory sealing of synapses around the conical CFNE shafts. The baseline and noise levels did not change when the whole active electrode area was inserted into the cleft and the limiting currents were restored to their original value after withdrawing CFNEs from synapses. Altogether these successful tests ensured that in the next series of experiments any neurotransmitter fluxes detected by inserted CFNEs arose from within the synapses and that the insertion process did not affect the surface of CFNEs or their sensitivity.

After insertion of CFNEs in synapses, and elicitation of release by high-K^+ solution puffs, well-defined quantal amperometric spikes were recorded in ca. 48% of cases (Figure 3a). Amperometric peaks displaying two distinct characteristics were recorded. Approximately 42% of spikes, termed hereafter "simple" events, exhibited a single rising phase followed by a single falling one (Figure 3a,c) being well-separated in time (ca. 40 ms average separation) from the previous and next release events. Their average amplitude (I_{max}), durations ($t_{1/2}$), and number of released molecules were 7.64 ± 0.32 pA, 0.53 ± 0.01 ms, and $1.77 \pm 0.16 \times 10^4$ molecules, respectively. The remaining 58% of events, termed "complex events", consisted in sequences of typically 2 to 5 sub-spikes (only 10% displayed more than 5 sub-spikes) with overall longer durations ($t_{1/2}^{complex} = 2.90 \pm 0.13$ ms, Figure 3b,d,e) and more released molecules ($3.98 \pm 0.37 \times 10^4$ molecules) than that of single events. Each of such sequence was separated from the previous or following release events by a 40 ms average time as observed as for single events. Within a given sequence, the sub-spikes exhibited well-defined rising and falling phases with smaller $t_{1/2}^{sub}$ values than for single events (Figure 3a) and were separated by 2 ms ($\Delta t_{sub} = 2.30 \pm 0.18$ ms, Figure 3b) from the previous or following one of the same sequence. Statistical analyses based on the mean separation time between simple events[14] could not accommodate the high frequency occurrence of so small time delays between sub-spikes of complex ones.

Furthermore, their current peak distribution was bimodal in opposition to the near-Gaussian current distribution of simple events (Figure 3f). Altogether, such unique properties of complex events clearly characterize them as belonging to an entirely different class than single ones, thus evidencing that different types of vesicle fusion modes co-exist inside synapses as reported for gland cells.[15,16]

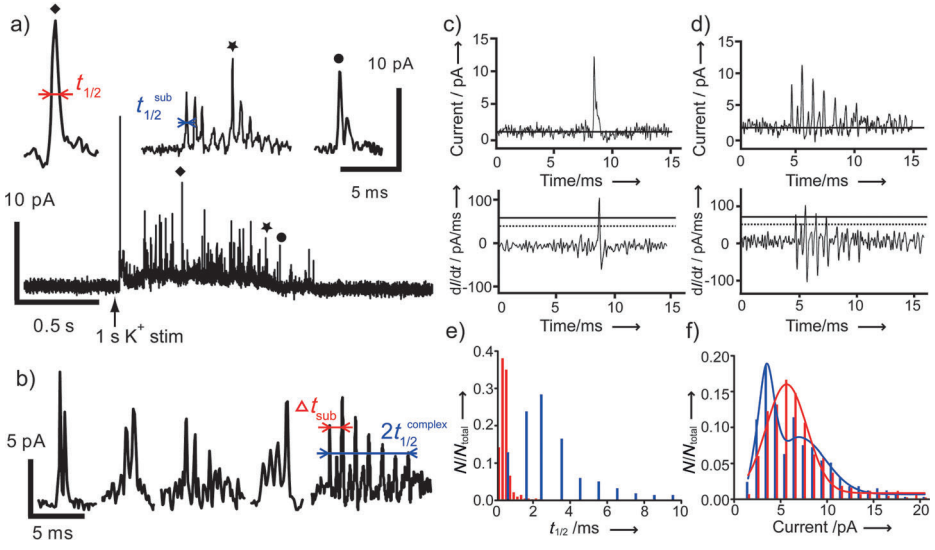

Figure 3. Nanoelectrode amperometry inside synapse between SCG neurons to monitor vesicular exocytosis. a) High K^+-induced amperometric spike and two complex events were amplified above; b) Representative examples of complex events; c,d) the upper panel shows examples of a simple and a complex amperometric current trace; the lower panels show the first derivative (dI/dt) of the current. The solid and dotted lines are threshold of 3.0×rms noise and 5.0×rms noise respectively; e,f) Histograms of simple (red) versus complex (blue) events characteristics in $t_{1/2}$(n=400 simple events and n=532 complex events) and peak heights (n=433 simple events and n=544 complex events).

In another series of experiments we compared events detected with one CFNE inserted inside a synapse to those simultaneously detected with another CFNE placed on the top of the corresponding varicosity in a "semi-artificial synapse" configuration (Figure 4a,b). Current spikes recorded simultaneously at both electrodes exhibited fully distinctive features (Figure 4c). Detection probabilities, exocytosis frequencies and complex events detection percentage drastically differed between the two positions. Among the 110 dual-electrode 100 seconds recordings performed, 48.2% evidenced current spikes were recorded from inside synapses, while only 24.5% could be detected from above (Figure 4d); furthermore, in average, 32.7 ± 5.7 current spikes were detected inside synapses while only 4.8 ± 1.4 were recorded above (Figure 4e); in addition, 58% of detected events were complex ones inside synapses while this was only 13% above synapses. Although these simultaneous comparisons confirmed the reality of release from varicosities top areas,[12b,13] the different characteristics observed validates the non-uniform distribution of active release zones, and the fact that they obey different and unsynchronized processes. This definitively confirms that neurons display different vesicle fusion modes at different parts of their axon buttons. The synaptic membrane facing its postsynaptic target possesses more active hot spots[6] and gives rise to a larger amount of complex events.

To evaluate the scope of the method, neuromuscular synapses were also investigated (Figure S7, and Movie S2). Amperometric spikes evoked by high-K^+ solution evidenced high percentage of complex events (52.3% of 459 events

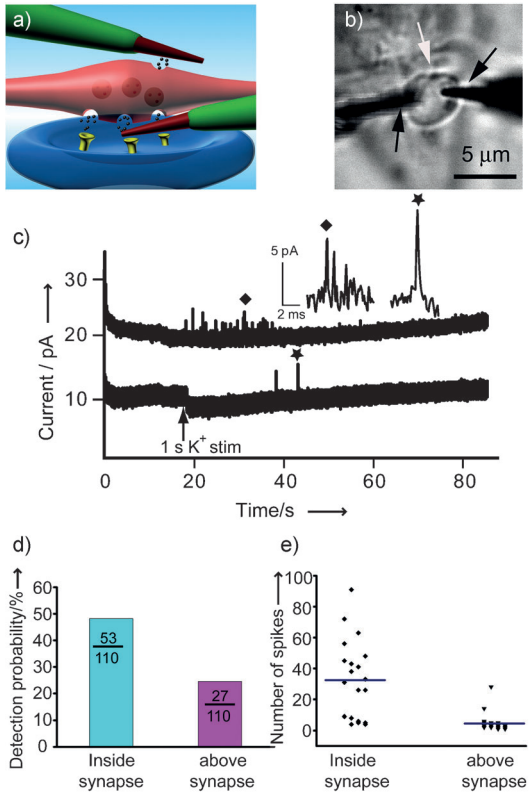

Figure 4. Simultaneous monitoring of vesicular exocytosis under "semi-artificial synapse" and "inside synapse" configurations with two CFNEs. a,b) Schematic diagram (a) and photomicrograph (b) showing two CFNEs (black arrows, the left one inside the synapse and the right one on the top of the synapse) to simultaneously detect vesicular exocytosis from basal and apical pole of a single varicosity (white arrow). c) Quantal amperometric spikes, the upper and bottom traces represent current spikes recorded on the electrodes inside the synapse and at the apical pole. d,e) Histograms of detection probability (d) and scatter plot showing the distribution of spikes number detected during 100 s recording (e) at the two configurations.

recorded) (Figure S8a,b). Overall the characteristics of the detected events were very similar to those described above for SCG-SCG synapses: complex events showed longer durations ($t_{1/2}{}^{complex} = 1.77 \pm 0.10$ ms) than simple ones ($t_{1/2} = 0.39 \pm 0.02$ ms, Figure S8c) and a bimodal current spike distribution was again observed for complex events while single ones displayed a classical near-Gaussian distribution (Figure S8d). This demonstrate that CFNE-amperometry has broad application range for monitoring and characterizing neurotransmitter release inside synaptic clefts and therefore offers an excellent procedure for better understanding of synaptic communication.

In summary, we developed a nanoelectrode-based amperometric method for direct monitoring vesicular exocytosis occurring inside individual synapses with high spatiotemporal resolution in real time. The versatility and importance of this new tool and method has been demonstrated by real-time monitoring inside neuronal junctions and neuromuscular junctions. Of particular importance is that these results have established that a large percentage (>50%) of exocytotic events involved complex sequence of events totally distinct from the usual single spike events detected by amperometry with CFMEs at endocrine cells. Though, the biological mechanisms underlying the occurrence of these complex events remain to be elucidated, complex events features are very suggestive of "Kiss and Run" ones (K&R).[15,16] Indeed, if transposed to amperometry, K&R features observed with patch-clamp[15] are expected to lead to sequences of complex spikes as those observed in this work. Though this is currently investigated in our joint team, our present results demonstrate that this is a major mode of fusion for NE release inside SCG synapses. In addition, the above results directly confirm that the active release zones in synaptic buttons are mostly concentrated in the regions facing the postsynaptic targets. Though, less active ones located outside the cleft release apparently without any synchronization.

The perfect ability of this new amperometric method to monitor and quantify neurotransmitter release in real time directly inside single synapses is expected to allow overcoming several previous limitations and offering a better understanding of the true nature of neuronal communications.

Received: April 28, 2014
Revised: June 10, 2014
Published online: July 24, 2014

Keywords: amperometry · complex exocytosis · nanoelectrodes · neurotransmitters · synapses

[1] a) C. F. Stevens, *Neuron* **2003**, *40*, 381–388; b) E. D. Gundelfinger, M. M. Kessels, B. Qualmann, *Nat. Rev. Mol. Cell Biol.* **2003**, *4*, 127–139; c) T. C. Südhof, J. Rizo, *Cold Spring Harbor Perspect. Biol.* **2011**, *3*:a005637; d) V. Haucke, E. Neher, S. J. Sigrist, *Nat. Rev. Neurosci.* **2011**, *12*, 127–138.

[2] a) C. A. Kaiser, R. Schekman, *Cell* **1990**, *61*, 723–733; b) J. A. McNew, F. Parlati, R. Fukuda, R. J. Johnston, K. Paz, F. Paumet, T. H. Sollner, J. E. Rothman, *Nature* **2000**, *407*, 153–159; c) R. Fernández-Chacón, A. Konigstorfer, S. H. Gerber, J. Garcia, M. F. Matos, C. F. Stevens, N. Brose, J. Rizo, C. Rosenmund, T. C. Südhof, *Nature* **2001**, *410*, 41–49.

[3] a) M. Puopolo, S. E. Hochstetler, S. Gustincich, R. M. Wightman, E. Raviola, *Neuron* **2001**, *30*, 211–225; b) D. L. Robinson, A. Hermans, A. T. Seipel, R. M. Wightman, *Chem. Rev.* **2008**, *108*, 2554–2584; c) R. Jahn, D. Fasshauer, *Nature* **2012**, *490*, 201–207; d) A. A. Alabi, R. W. Tsien, *Annu. Rev. Physiol.* **2013**, *75*, 393–422; e) T. C. Südhof, *Neuron* **2013**, *80*, 675–690.

[4] a) R. M. Wightman, J. A. Jankowski, R. T. Kennedy, K. T. Kawagoe, T. J. Schroeder, D. J. Leszczyszyn, J. A. Near, E. J. Diliberto, Jr., O. H. Viveros, *Proc. Natl. Acad. Sci. USA* **1991**, *88*, 10754–10758; b) E. V. Mosharov, D. Sulzer, *Nat. Methods* **2005**, *2*, 651–658; c) A. Schulte, W. Schuhmann, *Angew. Chem.* **2007**, *119*, 8914–8933; *Angew. Chem. Int. Ed.* **2007**, *46*, 8760–8777; d) C. Amatore, S. Arbault, M. Guille, F. Lemaitre, *Chem. Rev.* **2008**, *108*, 2585–2621; e) Y. X. Huang, D. Cai, P. Chen, *Anal. Chem.* **2011**, *83*, 4393–4406; f) R. Trouillon, M. K. Passarelli, J. Wang, M. E. Kurczy, A. G. Ewing, *Anal. Chem.* **2013**, *85*, 522–542.

[5] a) H. J. Koester, D. Johnston, *Science* **2005**, *308*, 863–866; b) T. Branco, K. Staras, *Nat. Rev. Neurosci.* **2009**, *10*, 373–383; c) C. Eroglu, B. A. Barres, *Nature* **2010**, *468*, 223–231.

[6] T. C. Südhof, *Neuron* **2012**, *75*, 11–25.

[7] a) W. Z. Wu, W. H. Huang, W. Wang, Z. L. Wang, J. K. Cheng, T. Xu, R. Y. Zhang, Y. Chen, J. Liu, *J. Am. Chem. Soc.* **2005**, *127*, 8914 – 8915; b) Y. Takahashi, A. I. Shevchuk, P. Novak, Y. Zhang, N. Ebejer, J. V. Macpherson, P. R. Unwin, A. J. Pollard, D. Roy, C. A. Clifford, H. Shiku, T. Matsue, D. Klenerman, Y. E. Korchev, *Angew. Chem.* **2011**, *123*, 9812 – 9816; *Angew. Chem. Int. Ed.* **2011**, *50*, 9638 – 9642; c) P. Sun, F. O. Laforge, T. P. Abeyweera, S. A. Rotenberg, J. Carpino, M. V. Mirkin, *Proc. Natl. Acad. Sci. USA* **2008**, *105*, 443 – 448; d) Y. Wang, J. M. Noel, J. Velmurugan, W. Nogala, M. V. Mirkin, C. Lu, M. G. Collignon, F. Lemaitre, C. Amatore, *Proc. Natl. Acad. Sci. USA* **2012**, *109*, 11534 – 11539.

[8] a) X. T. Zheng, C. M. Li, *Chem. Soc. Rev.* **2012**, *41*, 2061 – 2071; b) S. T. Oja, M. Wood, B. Zhang, *Anal. Chem.* **2013**, *85*, 473 – 486.

[9] a) T. G. Strein, A. G. Ewing, *Anal. Chem.* **1992**, *64*, 1368 – 1373; b) J. A. Jankowski, T. J. Schroeder, E. L. Ciolkowski, R. M. Wightman, *J. Biol. Chem.* **1993**, *268*, 14694 – 14700; c) S. Arbault, P. Pantano, J. A. Jankowski, M. Vuillaume, C. Amatore, *Anal. Chem.* **1995**, *67*, 3382 – 3390; d) W. H. Huang, D. W. Pang, H. Tong, Z. L. Wang, J. K. Cheng, *Anal. Chem.* **2001**, *73*, 1048 – 1052.

[10] C. G. Zoski, M. V. Mirkin, *Anal. Chem.* **2002**, *74*, 1986 – 1992.

[11] a) J. A. Jankowski, K. T. Kawagoe, R. M. Wightman, C. Lefrou, C. Amatore, *Anal. Chem.* **1992**, *64*, 3077 – 3083; b) B. Zhang, M. L. A. V. Heien, M. F. Santillo, L. Mellander, A. G. Ewing, *Anal. Chem.* **2011**, *83*, 571 – 577; in agreement with lateral collection of neurotransmitters released by sites located beyond their contact area.

[12] a) R. Rees, R. P. Bunge, *J. Comp. Neurol.* **1974**, *157*, 1 – 11; b) Z. Zhou, S. Misler, *Proc. Natl. Acad. Sci. USA* **1995**, *92*, 6938 – 6942.

[13] a) D. S. Kon, B. Hille, *Proc. Natl. Acad. Sci. USA* **1997**, *94*, 1506 – 1511; b) Z. Chiti, A. G. Teschemacher, *FASEB J.* **2007**, *21*, 2540 – 2550.

[14] For the statistical method used see: C. Amatore, S. Arbault, Y. Bouret, M. Guille, F. Lemaître, Y. Verchier, *Anal. Chem.* **2009**, *81*, 3087 – 3093.

[15] For characterization of Kiss and Run by patch-clamp, see e.g.: a) E. Neher, *Nature* **1993**, *363*, 497 – 498; b) A. W. Henkel, H. Meiri, H. Horstmann, M. Lindau, W. Almers, *EMBO J.* **2000**, *19*, 84 – 93; c) L. J. Breckenridge, W. Almers, *Nature* **1987**, *328*, 814 – 817; d) A. E. Spruce, L. J. Breckenridge, A. K. Lee, W. Almers, *Neuron* **1990**, *4*, 643 – 654.

[16] For characterization of Kiss and Run by amperometry, see e.g.: a) R. G. W. Staal, E. V. Mosharov, D. Sulzer, *Nat. Neurosci.* **2004**, *7*, 341 – 346; b) R. M. Wightman, C. L. Haynes, *Nat. Neurosci.* **2004**, *7*, 321 – 322; c) L. J. Mellander, R. Trouillon, M. I. Svensson, A. G. Ewing, *Sci. Rep.* **2012**, *2*, 907; d) J. T. Liu, L. S. Hu, Y. L. Liu, R. S. Chen, Z. Cheng, S. J. Chen, C. Amatore, W. H. Huang, K. F. Huo, *Angew. Chem.* **2014**, *126*, 2681 – 2685; *Angew. Chem. Int. Ed.* **2014**, *53*, 2643 – 2647.

